Physics and Chemistry of Minerals (2024) 51:11
https://doi.org/10.1007/s00269-024-01271-y

ORIGINAL PAPER

# Pressure-induced large volume collapse and possible spin transition in HP-$PdF_2$-type $FeCl_2$

Yao Yao[1,2,3] · Xi Liu[1,3] · Xueyan Du[2] · Lili Zhang[4] · Hongsheng Yuan[2]

Received: 26 December 2023 / Accepted: 14 February 2024 / Published online: 1 April 2024


## Abstract

Iron hydroxide $FeO_2H_x$ ($x \leq 1$) and ferrous iron chloride $FeCl_2$ can adopt the HP-$PdF_2$-type (space group: $Pa\bar{3}$, $Z=4$) structure in the lowermost mantle, potentially contributing to the geochemical cycles of hydrogen and chlorine within Earth's deep interior, respectively. Here we investigate the high-pressure behavior of HP-$PdF_2$-type $FeCl_2$ by X-ray diffraction (XRD) and Raman measurements in laser-heated diamond anvil cells. Our results show that HP-$PdF_2$-type $FeCl_2$ can be formed at 60–67 GPa and 1650–1850 K. Upon cold decompression, the diffraction peaks at pressures above 10 GPa can be indexed to the HP-$PdF_2$-type structure. Intriguingly, the calculated cell volumes reveal a remarkable decrease of $\Delta V / V = \sim 14\%$ between 36 and 40 GPa, which is possibly caused by a pressure-induced spin transition of $Fe^{2+}$ (HS: high-spin → LS: low-spin). We also observe distinct changes in Raman spectra at 33–35 GPa, practically coinciding with the onset pressures of isostructural phase transition in XRD results. Our observations combined with previous studies conducted at megabar pressures suggest that HP-$PdF_2$-type $FeCl_2$, with a wide pressure stability range, if present in subducting slabs, could facilitate the transport of chlorine from the middle lower mantle to the outer core.

**Keywords** HP-$PdF_2$-type $FeCl_2$ · High pressure · X-ray diffraction · Raman spectroscopy · Spin transition · Equation of state

## Introduction

Previous mass balance calculations have revealed an excess of chlorine (Cl) inputs over outputs in certain subduction zones (Barnes and Straub 2010; John et al. 2011), suggesting a dynamic balance in the Cl geochemical cycle. To gain a deeper understanding of Cl storage, distribution, and budget on Earth, it is essential to analyze Cl in various Earth reservoirs (Frezzotti and Ferrando 2018). Serpentinites play a crucial role in the recycling of hydrogen (H) and Cl through slab subduction (Scambelluri and Philippot 2001). Notably, unusual nano-inclusions containing NaCl, $CaCl_2$, KCl, and $PbCl_2$ chlorides have been discovered in diamonds originating from the transition zone (Wirth et al. 2009). Roberge et al. (2017) demonstrated that hydrous wadsleyite and ringwoodite can contain approximately 100 ppm Cl, suggesting that the transition zone could be a significant Cl reservoir. Recent high pressure-temperature experimental studies have demonstrated that chemical reactions can occur in Fe-, Cl-containing systems, including both wet $Mg_{0.6}Fe_{0.4}SiO_3$–NaCl–$H_2O$ and $FeO_2H$–NaCl and dry FeO–KCl systems, producing a HP-$PdF_2$-type (space group: $Pa\bar{3}$, $Z=4$) $FeCl_2$ phase (Koemets et al. 2020; Yin et al. 2022; Yuan et al. 2022). Ab initio calculations also predict the formation of this $FeCl_2$ phase under extreme conditions (Du et al. 2018; Yuan et al. 2022). These findings indicate that the HP-$PdF_2$-type $FeCl_2$ may serve as a potential host for Cl in the lower mantle and even the outer core.

Rozenberg et al. (2009) showed that $FeCl_2$ exhibits two electronic phase transitions upon cold compression, maintaining a hexagonal $CdI_2$-type (space group: $P\bar{3}m1$, $Z=1$) structure from ~0.6 GPa to 65 GPa. The transitions first start at a low-pressure phase (LP), then pass through an

✉ Hongsheng Yuan
hongsheng.yuan@hpstar.ac.cn

1 School of Earth and Space Sciences, Peking University, Beijing 100871, China

2 Center for High Pressure Science and Technology Advanced Research (HPSTAR), Shanghai 201203, China

3 Key Laboratory of Orogenic Belts and Crustal Evolution, Ministry of Education of China, Beijing 100871, China

4 Shanghai Institute of Applied Physics, Chinese Academy of Sciences, Shanghai 201204, China

intermediate phase (IP) between 30 and 57 GPa, and eventually reach a high-pressure phase (HP) at pressures greater than 32 GPa. The LP-IP interface shows no volume change, but exhibits a discontinuous shrinkage of *a* axis and an increase of *c* axis, which is attributed to the quenching of the orbital term. The subsequent IP-HP transition shows a decrease in Fe-Cl bond length and an abrupt volume decrease of $\Delta V / V = \sim 3.5\%$, accompanying with a breakdown of the charge-transfer correlation. Note that no spin transitions are involved in these two pressure-induced electronic transitions.

The spin transition of iron holds fundamental significance for mantle physics, as it impacts the density, elasticity, element partitioning and transport properties of major mantle minerals (Lin et al. 2013; Badro 2014). Recent studies demonstrated that $FeO_2$ and $FeO_2H_x$ ($x \leq 1$) phases might exist in the deep lower mantle, potentially accounting for the global oxygen-hydrogen cycles (Hu et al. 2016; Liu et al. 2017; Mao et al. 2017; Nishi et al. 2017; Yuan et al. 2018). These unique iron oxide-hydroxide compounds were initially thought to be related to the pyrite structure, while the latest single-crystal X-ray diffraction data indicated they align more closely with the HP-$PdF_2$-type structure (Koemets et al. 2021). X-ray emission spectroscopy experiments indicated that HP-$PdF_2$-type $FeO_2$ and $FeO_2H_x$ ($x \leq 1$) undergo high- to low- spin transitions at around 50–65 GPa (Jang et al. 2019; Liu et al. 2019). Determining the volume reduction caused by the spin transition in $FeO_2H_x$ ($x \leq 1$) is challenging, primarily because of the pressure-dependent dehydrogenation contribution and the varying H content *x*, which can result in a volume difference of up to 10.7% (Hu et al. 2017). As an Fe analogue to $FeO_2$ and $FeO_2H_x$ ($x \leq 1$) phases, the HP-$PdF_2$-type $FeCl_2$ may provide new insight into this issue. In this study, we have explored the high-pressure behavior of HP-$PdF_2$-type $FeCl_2$ by X-ray diffraction (XRD) and Raman measurements.

## Experimental methods

### Starting materials and sample preparation

Symmetric diamond anvil cells (DAC) with culet diameters of 250 μm were used for the high pressure and temperature experiments. A cavity with a diameter of ~ 100 μm was laser-drilled into a rhenium gasket indented to 30 μm thickness to create the sample chamber. We used anhydrous $FeCl_2$ (99% purity; Aladdin chemicals) as the starting material. Sample preparation was carried out in a glove box due to the high deliquescence of the $FeCl_2$. A thin $FeCl_2$ foil, approximately 10 μm in thickness, was carefully situated on pre-installed silica spacers to avoid the direct contact with the diamond surface. The sample assembly was sealed in DAC in the glove box and transferred to a gas-loading system (HPSTAR). Ne was then loaded as a thermal insulator, pressure medium and pressure calibrant.

### Laser heating

Samples were compressed to target pressures at room temperature. Then we heated the samples to target temperatures for about 15 min, using a double-sided 1070-nm Ytterbium fiber laser heating system at HPSTAR (Liu et al. 2022; Yang et al. 2023). The heating temperature was determined by fitting the visible portion of the gray-body radiation from both sides of the heated sample to the Planck radiation function. The accuracy of these fittings was precise, yielding errors within a narrow range of 5 to 10 K. The discrepancy in temperature between the two sides of the sample did not exceed 50 K. To ensure stability throughout the heating experiment, the laser power on each side of DAC was meticulously adjusted, thereby restricting temperature fluctuations to ± 100 K. Hereafter, we use this value to describe the temperature uncertainty.

### Synchrotron X-ray diffraction (XRD)

Synchrotron XRD experiments at high pressure and room temperature were carried out at the 15U1 beamline of Shanghai Synchrotron Radiation Facility (Zhang et al. 2015). The wavelength of the incident X-ray beam was 0.6199 Å and the beam size was about $5 \times 5$ μm$^2$. Pressures were determined by the equation of state (EoS) of Ne medium (Fei et al. 2007). Diffraction data were collected in about 1–4 GPa steps on decompression. An exposure time of 10 s was used for every pattern at each pressure. The collected XRD images were calibrated with a $CeO_2$ standard and then integrated to 2$\theta$-intensity patterns using the program DIOPTAS (Prescher and Prakapenka 2015). Unit-cell parameters were refined by nonlinear regression methods using the software UNITCELL (Holland and Redfern 1997) using 6 most intense diffraction peaks.

### High-pressure Raman spectroscopy

Raman spectra were collected using a Renishaw Raman spectrometer. Samples were excited by a 532 nm wavelength laser with a holographic notch filter. The matching grating was 2400 l/mm and the maximum output laser power was 50 mW. The system was calibrated before our high-pressure measurements using the Raman peak of a reference Si crystal at 520 cm$^{-1}$. The spectra of our samples were collected in the wavenumber ranges of 50–1000 cm$^{-1}$ with an exposure time of 100 s and 4 accumulations. Pressures

were determined based on the Raman shift of diamond edge (Akahama and Kawamura 2006).

## Results and discussion

### Synthesis of HP-$PdF_2$-type $FeCl_2$

By comparing the Raman spectra of the sample before and after laser heating, we can verify whether a possible chemical reaction or a phase transition has occurred. As suggested by Rozenberg et al. (2009), the sample above 57 GPa transforms into a high-pressure hexagonal (HP) phase upon cold compression. As shown in Fig. 1a, two Raman modes can be clearly observed at pressures ranging from 59.8 to 65.9 GPa (i.e., ~417 and ~508 $cm^{-1}$ at ~65.9 GPa), which can be attributed to the $CdI_2$-type HP phase according to the study of Rozenberg et al. (2009). At 59.8 GPa after heating up the sample at 1650(100) K, we observed the appearance of a new peak around 318 $cm^{-1}$, while the Raman modes of the HP phase were still the dominant. Upon increasing the pressure to 61.2 GPa and heating the sample to 1850(100) K, we could only detect this new Raman peak, indicating the formation of a new phase at the expense of the HP phase. This phenomenon was reproduced in another run at 65.9 GPa after annealing. For this run, we collected a two-dimensional (2D) Raman mapping data in a 50×40 $\mu m^2$ area with a 2 μm step size. As shown in Fig. 1b, the new

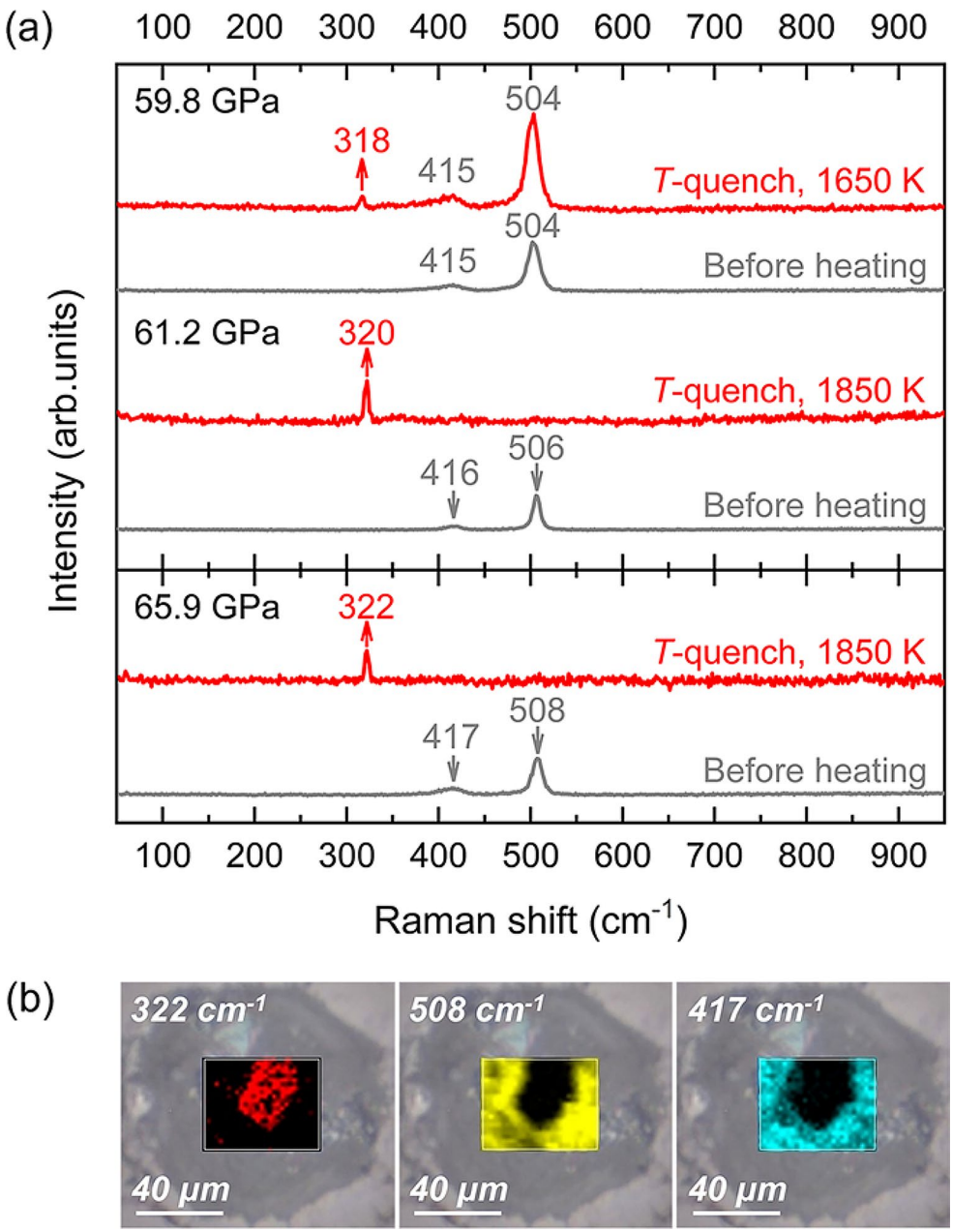


**Fig. 1** (**a**) Raman spectra before and after laser heating at typical pressures. Gray lines: spectra before laser heating. Red lines: spectra after laser heating. (**b**) Raman modes distribution at 65.9 GPa based on two-dimensional Raman mapping results

peak was located in the heating center, while the characteristic peaks of the HP phase were distributed in the unheated region. Furthermore, the Raman spectra of the $CdI_2$-type HP phase at 55 GPa remained consistent before and after undergoing comparable laser heating annealing, indicating that a threshold pressure of approximately 60 GPa is necessary to initiate the transition to HP-$PdF_2$-type $FeCl_2$ phase.

Synchrotron XRD measurements were further conducted on the sample at 65.9 GPa after annealing. As the laser spot size of ~20 μm in diameter is larger than the X-ray spot size of ~5 μm in diameter, we can collect the XRD data of the heated center area without the HP phase. As seen in Fig. 2, except for the diffractions of Ne medium and Re gasket, all peaks in the XRD pattern can be well indexed by a cubic $Pa\bar{3}$ lattice with $a = 5.1353(6)$ Å and $V = 135.43(5)$ Å$^3$, indicating the formation of pure HP-$PdF_2$-type $FeCl_2$. The synthesis pressure is much lower than megabar pressures in previous studies (Koemets et al. 2020; Yin et al. 2022; Yuan et al. 2022).

## Decompression XRD experiments

We performed decompression XRD experiments on HP-$PdF_2$-type $FeCl_2$ at room temperatures (Fig. 2–4). Even

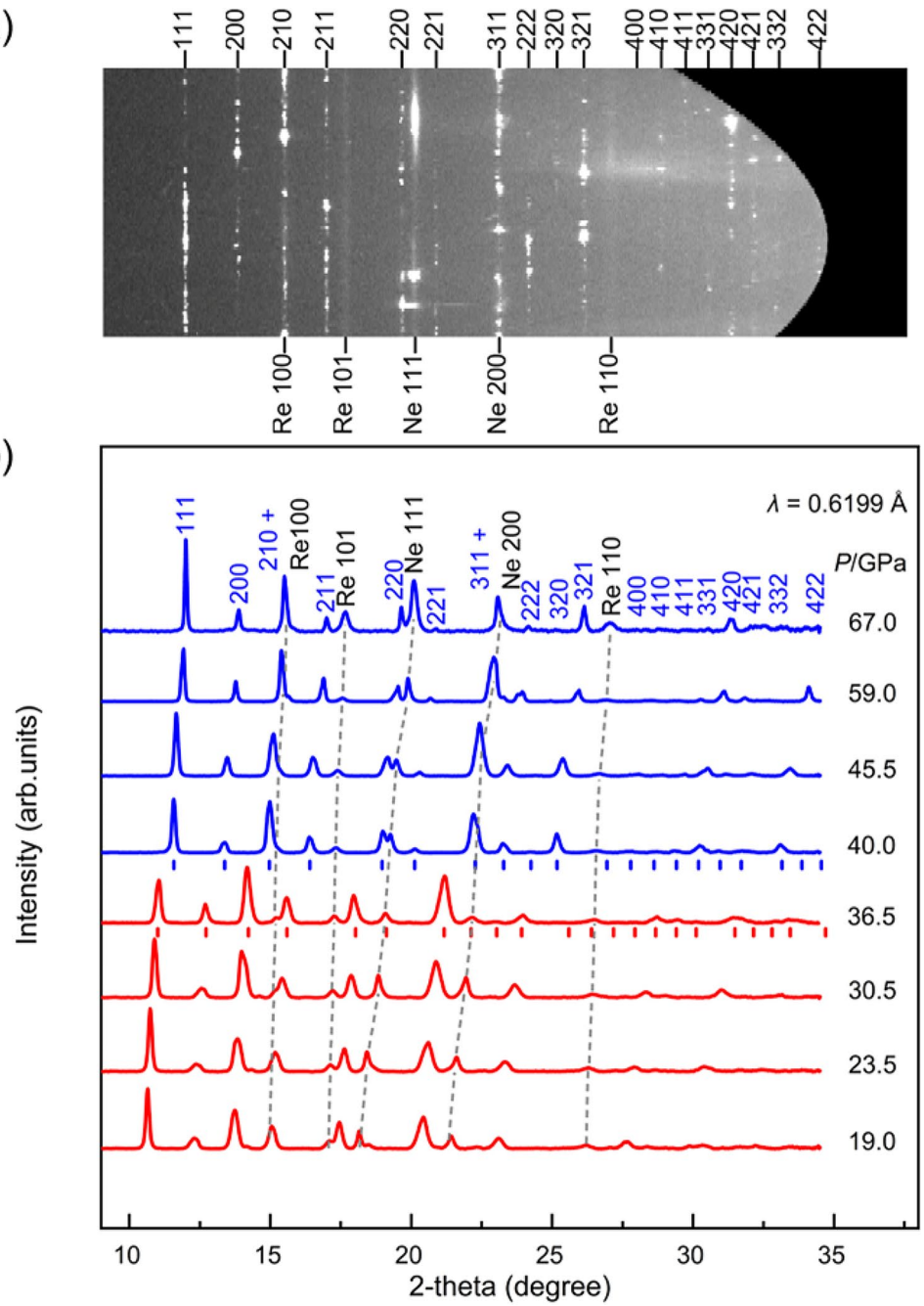


**Fig. 2** Typical high-pressure X-ray diffraction (XRD) patterns of HP-$PdF_2$-type $FeCl_2$ at room temperature. (**a**) A two-dimensional XRD image at 67.0 GPa. (**b**) Integrated 2$\theta$-intensity XRD patterns during decompression. Blue and red lines denote the low-spin and high-spin states, respectively. Small vertical bars beneath the relevant patterns signify the indexing of the diffraction peaks associated with the HP-$PdF_2$-type $FeCl_2$. Grey dashed lines serve as visual aids for tracking the evolution of the diffraction peaks for neon (Ne) and rhenium (Re) under varying pressures

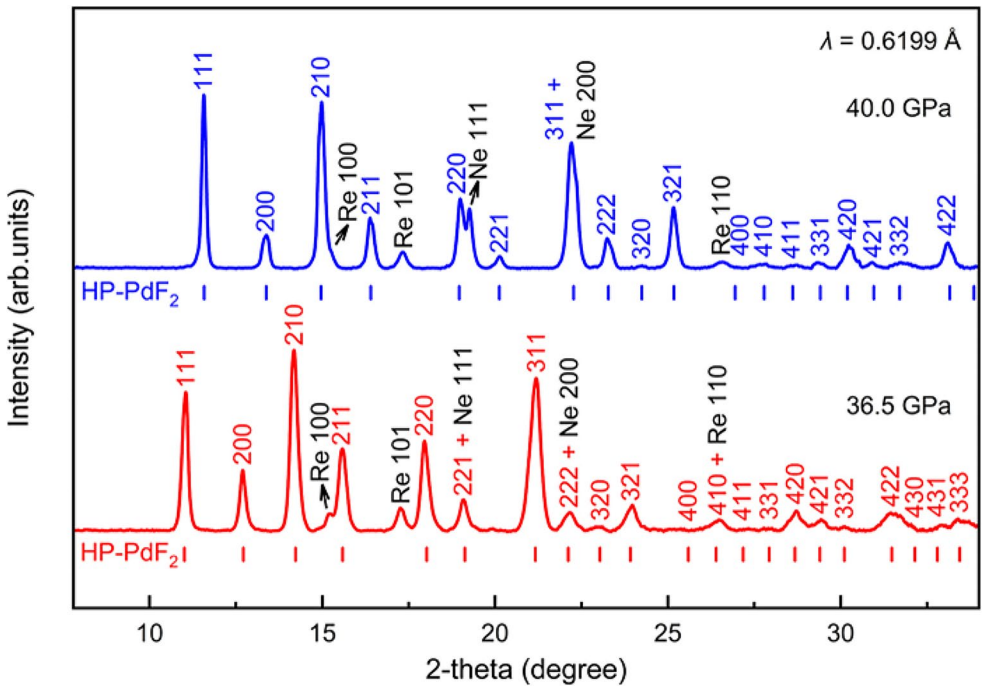


**Fig. 3** Indexing of the diffraction peaks associated with the HP-$PdF_2$-type $FeCl_2$ at 40.0 and 36.5 GPa. Blue and red lines denote the low-spin and high-spin states, respectively

**Table 1** The cell parameters of HP-$PdF_2$-type $FeCl_2$ phase at high pressures during decompression

| Pressure (GPa) | *a* (Å) | Volume (Å$^3$) |
|---|---|---|
| 67.0(5) | 5.1353(6) | 135.43(5) |
| 65.5(5) | 5.1373(4) | 135.58(3) |
| 65.0(5) | 5.1394(4) | 135.75(3) |
| 64.0(5) | 5.1473(5) | 136.37(4) |
| 63.0(5) | 5.1490(4) | 136.51(3) |
| 62.0(5) | 5.1687(5) | 137.29(4) |
| 61.5(5) | 5.1597(4) | 137.37(3) |
| 60.5(5) | 5.1636(4) | 137.68(3) |
| 59.0(5) | 5.1734(5) | 138.46(4) |
| 57.0(5) | 5.1967(6) | 140.34(5) |
| 53.0(5) | 5.2263(5) | 142.75(4) |
| 52.5(5) | 5.2288(5) | 142.96(4) |
| 51.5(5) | 5.2348(6) | 143.45(5) |
| 50.0(5) | 5.2454(5) | 144.32(4) |
| 45.5(5) | 5.2793(6) | 147.14(5) |
| 43.0(5) | 5.3001(6) | 148.88(5) |
| 40.0(5) | 5.3218(6) | 150.72(5) |
| 36.5(5) | 5.5936(5) | 175.02(5) |
| 35.5(5) | 5.5973(5) | 175.36(5) |
| 31.0(5) | 5.6518(7) | 180.53(6) |
| 30.5(5) | 5.6562(5) | 180.96(5) |
| 29.0(5) | 5.6747(6) | 182.74(6) |
| 28.5(5) | 5.6785(5) | 183.10(5) |
| 26.0(5) | 5.7095(6) | 186.12(6) |
| 23.5(5) | 5.7335(6) | 188.48(6) |
| 21.0(5) | 5.7667(5) | 191.77(5) |
| 19.0(5) | 5.7904(6) | 194.15(6) |

though non-hydrostatic conditions arising during cold decompression can cause broadening of the diffraction peaks, we successfully indexed the HP-$PdF_2$-type structure across a wide pressure range of 19–67 GPa in all diffraction patterns. As will be discussed later in Raman results, HP-$PdF_2$-type $FeCl_2$ is stable down to a pressure of ~10 GPa. When the sample is decompressed to about 6 GPa, its diffraction peaks can be indexed to a hexagonal lattice ($a = 3.5563(7)$ Å, $c = 5.547(4)$ Å), which is consistent with the $CdI_2$-type LP phase in the cold compression experiments (Rozenberg et al. 2009).

Notably, between 40 and 36.5 GPa during decompression, we found an abrupt shift in the diffraction peaks, suggestive of an isostructural phase transition (Fig. 3). Further analysis of the pressure-volume relationship revealed a sharp volume discontinuity with a pronounced change amounting to 14.3% (Table 1; Fig. 4). Such a significant change in volume—characterized by a marked collapse upon compression or a substantial expansion upon decompression—is likely due to a pressure-induced spin transition of $Fe^{2+}$ from a high-spin (HS) to a low-spin (LS) state, or vice versa. Spin transition of iron has been observed in other Fe-bearing minerals, such as siderite ($FeCO_3$) and $CaFe_2O_4$, where 6-fold coordinated iron is $Fe^{2+}$ and $Fe^{3+}$, respectively (Lavina et al. 2009; Merlini et al. 2010). Specifically, $FeCO_3$ and $CaFe_2O_4$ undergo pressure-induced isostructural HS-LS transitions at 43 and 50 GPa, with volume decreases of $\Delta V / V = 10\%$ and 8.4%, respectively (Lavina et al. 2009; Merlini et al. 2010). We denoted the HP-$PdF_2$-type $FeCl_2$ phase before the volume collapse as the HS state, and that after the volume collapse as the LS state. It can be expected

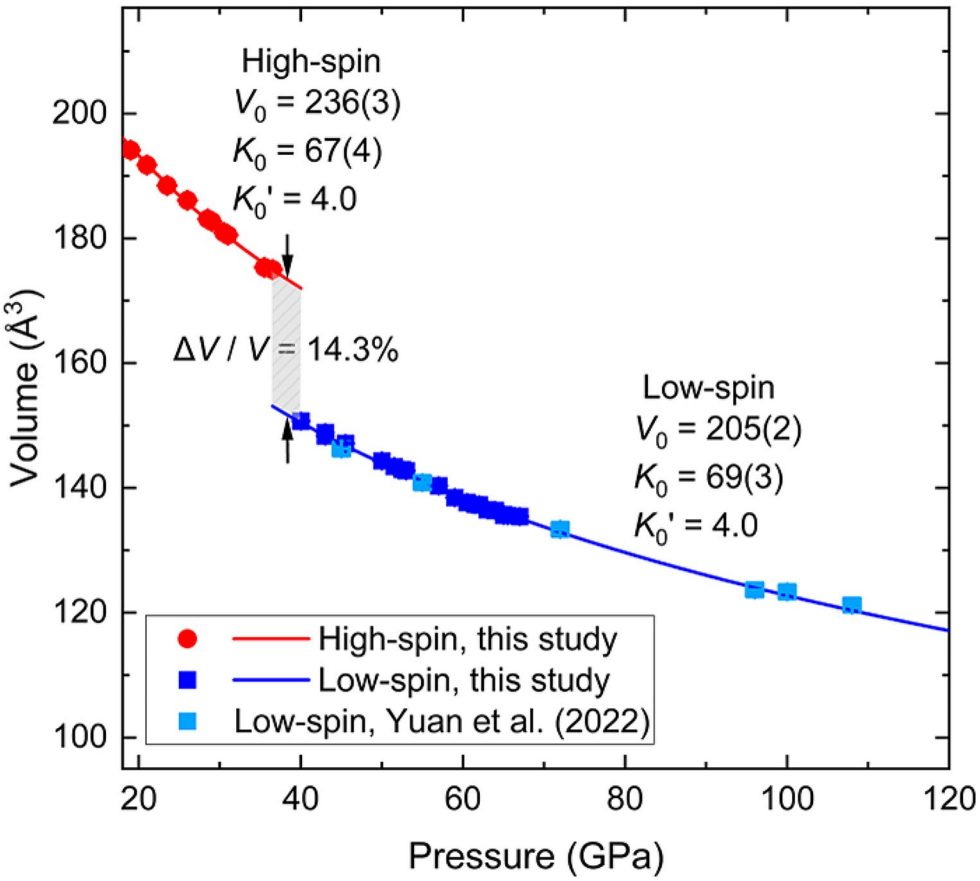


**Fig. 4** Cell volumes of HP-$PdF_2$-type $FeCl_2$ at high pressures. Red circles: data of the high-spin state, this study. Blue squares: data of the low-spin state, this study. Light blue squares: data from Yuan et al. (2022). Solid lines: fitted results using the second-order Birch-Murnaghan equation of state (BM-EoS). The pressures in this study were determined by the EoS of Ne (Fei et al. 2007), and the pressures in Yuan et al. (2022) were determined by the EoS of NaCl or Au (Fei et al. 2007)

that future high-pressure X-ray emission spectroscopy and Mössbauer spectroscopy studies will help to characterize the spin configuration of iron.

We fitted the second order Birch-Murnaghan equation to the pressure-volume data. We yielded $K_0 = 67(4)$ GPa and $V_0 = 236(3)$ Å$^3$ for the HS state. For the LS state, data from Yuan et al. (2022) were also included. As a result, we yielded $K_0 = 69(3)$ GPa and $V_0 = 205(2)$ Å$^3$ for the LS state. Therefore, the compressibilities of the HS and LS states are comparable in HP-$PdF_2$-type $FeCl_2$.

## Raman spectroscopy

We have demonstrated the effective utilization of Raman spectra for identifying $CdI_2$-type HP phase and HP-$PdF_2$-type phase of $FeCl_2$ (Fig. 1). After the synthesis of HP-$PdF_2$-type $FeCl_2$, the Raman spectra during decompression have been recorded as well (Fig. 5).

The LS state of HP-$PdF_2$-type $FeCl_2$ has a characteristic Raman mode centered at ~322 cm$^{-1}$ (denoted as $V_{LS}$) at 65.9 GPa, its frequency progressively decreases with decreasing pressure to 34.8 GPa. After further decompression to 32.7 GPa, four new Raman modes emerge, which are centered at 251 cm$^{-1}$, 269 cm$^{-1}$, 350 cm$^{-1}$ and 385 cm$^{-1}$ (denoted as $V_{HS1}$, $V_{HS2}$, $V_{HS3}$, and $V_{HS4}$, respectively). It is intriguing to note that the onset pressure (~33–35 GPa) of the dramatic changes in Raman spectra coincides with the onset pressure (~36–40 GPa) of the abrupt volume collapse in XRD experiments. The slight pressure difference might be caused by the usage of different pressure calibrants. As there is no symmetry change in XRD results, it is reasonable to infer that the abrupt changes in Raman modes reflect the electronic spin transition.

Factor group analysis predicts five active Raman modes ($A_g + E_g + 3T_g$) for HP-$PdF_2$-type structure. To our best knowledge, Raman spectroscopy data is available for only two HP-$PdF_2$-type $AX_2$ compounds: $ZnF_2$ (Kurzydłowski et al. 2020) and $CoF_2$ (Barreda-Argüeso et al. 2013). For HP-$PdF_2$-type $ZnF_2$, all five predicted Raman modes have been observed and assigned by density functional theory (DFT) calculations (Kurzydłowski et al. 2020). In contrast, HP-$PdF_2$-type $CoF_2$ reveals only one Raman active mode, with two additional modes from the coexisting $CaCl_2$-type $CoF_2$ (Barreda-Argüeso et al. 2013). The discrepancy in the number of observed Raman modes for these two compounds may arise from variations in the $AX_6$ octahedra (such as compaction, deformation and distortion), which can affect the frequency and intensity of corresponding Raman modes. In the case of HP-$PdF_2$-type $FeCl_2$ examined in this study, a substantial change in the effective ionic radius of $Fe^{2+}$ is

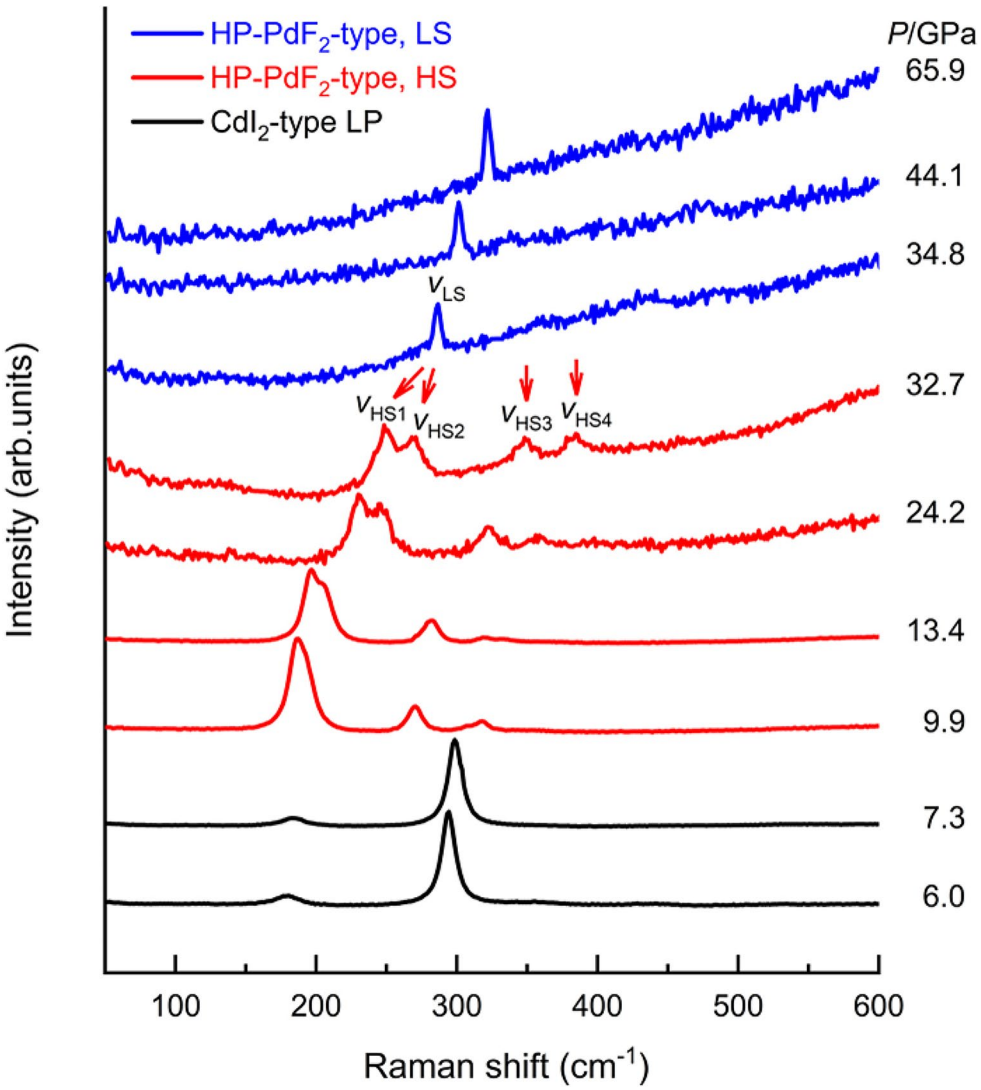


**Fig. 5** Representative Raman spectra of HP-$PdF_2$-type $FeCl_2$ and $CdI_2$-type LP phase during decompression at 300 K. HS: high-spin. LS: low-spin. The phase below ~7 GPa (black spectra) is assigned to $CdI_2$-type LP phase based on XRD results (Fig. 6)

expected as a result of transition from LS to HS state during decompression. These changes are likely to significantly alter the $FeCl_6$ octahedra, consequently impacting the frequency and intensity of the associated Raman modes. Advanced DFT calculations are expected to shed further light on this issue.

Indeed, significant changes in the Raman spectra have also been observed in $FeCO_3$ compound across its isostructural HS-LS transition, including the disappearance of the lattice mode L, discontinuous jumps of the lattice mode T and the internal vibration modes $v_1$ and $v_4$ to higher frequencies (Cerantola et al. 2015; Müller et al. 2016). In particular, the $v_1$ mode, which corresponds to the stretching vibration of the $CO_3^{2-}$ group, exhibits a high sensitivity to spin transitions. The change in the C–O bond lengths is directly influenced by the significant alteration in the radius of neighboring Fe atoms as they undergo a spin transition. The abrupt splitting or shifting of the $v_1$ mode therefore serves as a reliable indicator for detecting either a mixed-spin state or a sharply defined complete transition. For HP-$PdF_2$-type $FeCl_2$, the presence of mixed high-spin HS and LS states within a narrow pressure range of ~33–35 GPa is also possible based on Raman spectroscopy results.

Furthermore, the characteristic Raman spectra of the HS state of HP-$PdF_2$-type $FeCl_2$ can be traced back to approximately 10 GPa, suggesting the lower limit of pressure stability of the HS state at room temperature (Fig. 5). Below 10 GPa, it transforms to a pure $CdI_2$-type LP phase (Fig. 6), which has two distinctive Raman modes centered at 184 $cm^{-1}$ and 299 $cm^{-1}$ at 7.3 GPa. The pressure dependences of Raman shifts are linearly fitted for the $CdI_2$-type LP phase, HP-$PdF_2$-type HS and LS states, respectively (Fig. 7).

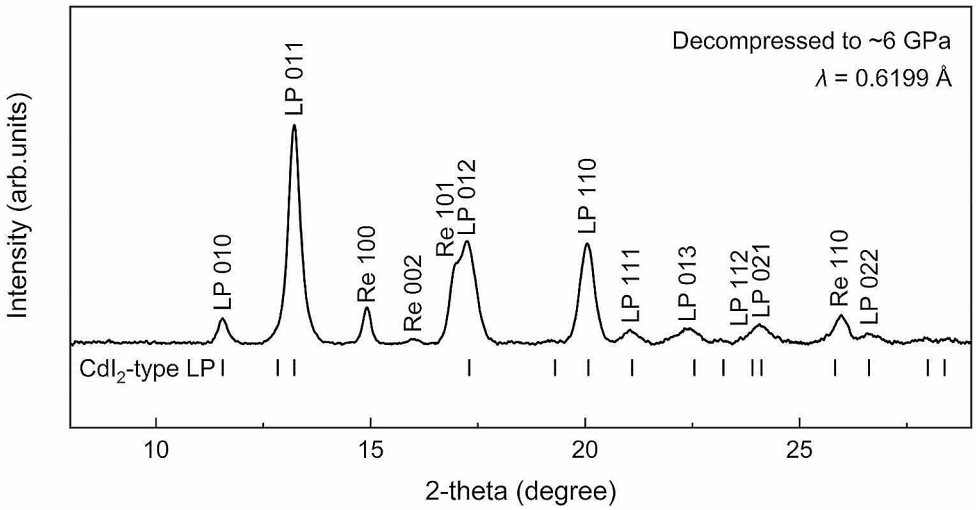


**Fig. 6** A representative XRD pattern of the $CdI_2$-type low-pressure phase (LP) of $FeCl_2$ obtained by decompression of HP-$PdF_2$-type $FeCl_2$ to ~6 GPa

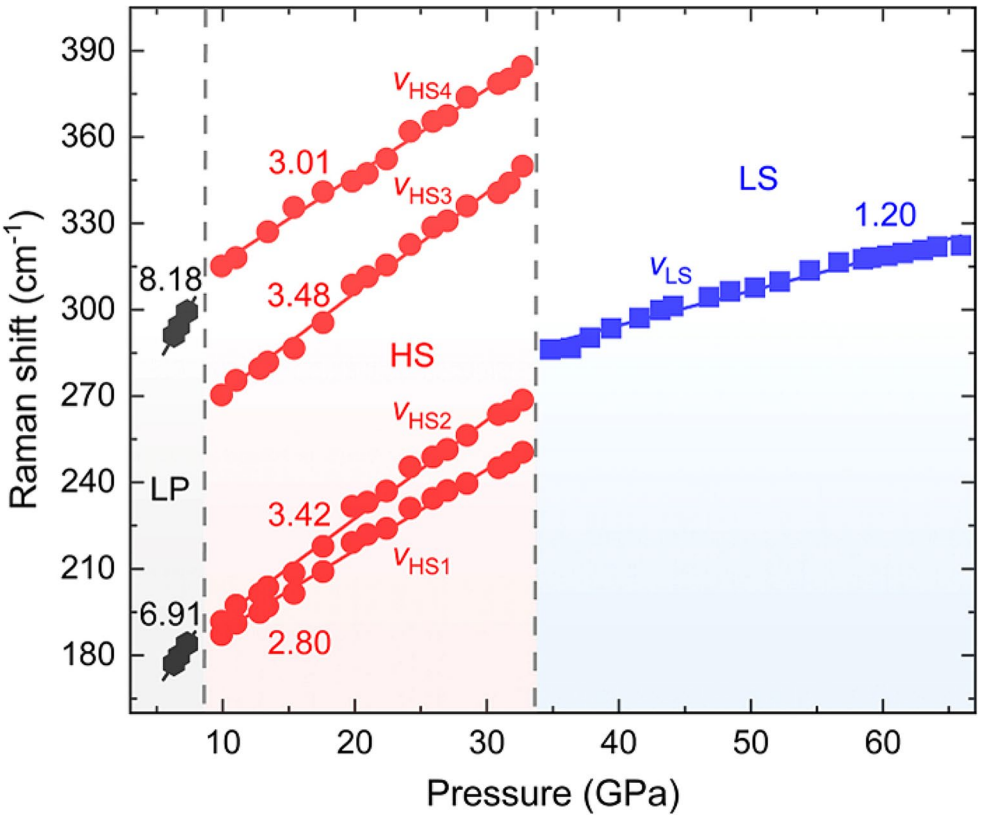


**Fig. 7** Pressure dependences of the Raman mode frequencies at room temperature. The black, red and blue lines are linear fittings for the $CdI_2$-type LP phase, HS state of HP-$PdF_2$-type $FeCl_2$ and LS state of HP-$PdF_2$-type $FeCl_2$, respectively. The pressure coefficients ($d\omega$ / $dP$) are also shown for the corresponding modes

## Comparison of HP-$PdF_2$-type $FeCl_2$, $FeO_2$ and $FeO_2H_x$ ($x \leq 1$)

The valence of Fe and O in HP-$PdF_2$-type $FeO_2$ and $FeO_2H_x$ ($x \leq 1$) continues to be a point of contention in both theoretical and experimental works (Streltsov et al. 2017; Boulard et al. 2019; Jang et al. 2019; Liu et al. 2019; Koemets et al. 2021). The main experimental challenge stems from the fact that the interpretation of high-pressure spectroscopic data relies predominantly on qualitative comparisons with standards that are either under ambient conditions or are sensitive to the structural environments (Boulard et al. 2019; Jang et al. 2019; Liu et al. 2019). For instance, Liu et al. (2019) interpreted their Mössbauer spectra of $FeO_2H_x$ ($x \leq 1$) and concluded that the iron was ferrous based on the standard samples of ferrous pyrite $FeS_2$, ferrous $Fe_{0.48}Mg_{0.52}O$, and ferric $Fe_2O_3$ under ambient conditions. On the contrary, Koemets et al. (2021) interpreted their Mössbauer spectra of the $Fe_{25}O_{32}$, Fe and $FeO_2$ mixture, identifying low-spin ferric iron in $FeO_2$. We suggest that ferrous $FeCl_2$ can serve as an appropriate standard to help solve this issue, because

it adopts the same HP-$PdF_2$-type crystallographic structure at high pressures, excludes mixed-valence substitutions, and potentially undergoes a pressure-induced spin transition.

## Conclusions

We have synthesized HP-$PdF_2$-type $FeCl_2$ at 60–67 GPa and 1650–1850 K in laser-heated DACs. Importantly, the decompression XRD results show an abrupt volume collapse of $\Delta V / V = \sim 14\%$ in HP-$PdF_2$-type $FeCl_2$ between 36 and 40 GPa, similar to previous observations in $FeCO_3$, suggesting a pressure-induced isostructural HS-LS transition. Meanwhile, dramatic changes in Raman modes can be observed at comparable pressures. Regarding the complex bonding nature and electronic structures in HP-$PdF_2$-type $FeO_2H_x$ ($x \leq 1$) and $FeO_2$, we suggest that HP-$PdF_2$-type $FeCl_2$ could be an effective standard for interpreting the high-pressure spectroscopic data of these compounds. Combined with previous studies, HP-$PdF_2$-type $FeCl_2$ phase is stable over a wide pressure range from 10 to 160 GPa at room temperature, and can serve as a stable Cl-host under pressure-temperature conditions of the middle lower mantle to the outer core.

**Acknowledgements** The authors acknowledge two anonymous reviewers whose detailed comments have greatly improved the quality of the manuscript. The authors are grateful for the financial support from the National Natural Science Foundation of China (Grants No.: 41902033, 42150103 and 42050203). The X-ray diffraction experiments were performed at beamline 15U1, Shanghai Synchrotron Radiation Facility.

**Author contributions** Yao Yao and Hongsheng Yuan contributed to the conception and design of the study. Methodology was performed by Yao Yao, Hongsheng Yuan, Xi Liu, Xueyan Du, and Lili Zhang. Formal analysis and investigation were performed by Yao Yao and Hongsheng Yuan. Data curation was performed by Yao Yao. The first draft of the manuscript was written by Yao Yao and Hongsheng Yuan. The original manuscript was subsequently reviewed and edited by Xi Liu, Xueyan Du, and Lili Zhang. Funding was acquired by Hongsheng Yuan. All authors have read and agreed to the published version of the manuscript.

**Data availability** No datasets were generated or analysed during the current study.

## Declarations

**Conflict of interest** The authors declare no competing interests.

## References

Akahama Y, Kawamura H (2006) Pressure calibration of diamond anvil Raman gauge to 310 GPa. J Appl Phys 100:1–4. https://doi.org/10.1063/1.2335683

Badro J (2014) Spin transitions in mantle minerals. Annu Rev Earth Planet Sci 42:231–248. https://doi.org/10.1146/annurev-earth-042711-105304

Barnes JD, Straub SM (2010) Chorine stable isotope variations in Izu Bonin tephra: implications for serpentinite subduction. Chem Geol 272:62–74. https://doi.org/10.1016/j.chemgeo.2010.02.005

Barreda-Argüeso JA, López-Moreno S, Sanz-Ortiz MN, Aguado F, Valiente R, González J, Rodríguez F, Romero AH, Muñoz A, Nataf L, Baudelet F (2013) Pressure-induced phase-transition sequence in $CoF_2$: an experimental and first-principles study on the crystal, vibrational, and electronic properties. Phys Rev B 88:1–15. https://doi.org/10.1103/PhysRevB.88.214108

Boulard E, Harmand M, Guyot F, Lelong G, Morard G, Cabaret D, Boccato S, Rosa AD, Briggs R, Pascarelli S, Fiquet G (2019) Ferrous iron under oxygen-rich conditions in the deep mantle. Geophys Res Lett 46:1348–1356. https://doi.org/10.1029/2019GL081922

Cerantola V, McCammon C, Kupenko I, Kantor I, Marini C, Wilke M, Ismailova L, Solopova N, Chumakov A, Pascarelli S, Dubrovinsky L (2015) High-pressure spectroscopic study of siderite ($FeCO_3$) with a focus on spin crossover. Am Mineral 100:2670–2681. https://doi.org/10.2138/am-2015-5319

Du X, Wang Z, Wang H, Iitaka T, Pan Y, Wang H, Tse JS (2018) Structures and stability of iron halides at the Earth's mantle and core pressures: implications for the missing halogen paradox. ACS Earth Sp Chem 2:711–719. https://doi.org/10.1021/acsearthspacechem.8b00034

Fei Y, Ricolleau A, Frank M, Mibe K, Shen G, Prakapenka V (2007) Toward an internally consistent pressure scale. Proc Natl Acad Sci 104:9182–9186. https://doi.org/10.1073/pnas.0609013104

Frezzotti ML, Ferrando S (2018) The role of halogens in the lithospheric mantle. In: Harlov DE, Aranovich L (eds) The role of halogens in terrestrial and extraterrestrial geochemical processes. Spinger Nature Ltd., Switzerland, pp 805–845. https://doi.org/10.1007/978-3-319-61667-4_13

Holland TJB, Redfern SAT (1997) Unit cell refinement from powder diffraction data: the use of regression diagnostics. Mineral Mag 61:65–77. https://doi.org/10.1180/minmag.1997.061.404.07

Hu Q, Kim DY, Yang W, Yang L, Meng Y, Zhang L, Mao H-K (2016) $FeO_2$ and FeOOH under deep lower-mantle conditions and Earth's oxygen–hydrogen cycles. Nature 534:241–244. https://doi.org/10.1038/nature18018

Hu Q, Kim DY, Liu J, Meng Y, Yang L, Zhang D, Mao WL, Mao H-K (2017) Dehydrogenation of goethite in Earth's deep lower mantle. Proc Natl Acad Sci 114:1498–1501. https://doi.org/10.1073/pnas.1620644114

Jang BG, Liu J, Hu Q, Haule K, Mao H-K, Mao WL, Kim DY, Shim JH (2019) Electronic spin transition in $FeO_2$: evidence for Fe(II) with peroxide $O_2^{2-}$. Phys Rev B 100:1–7. https://doi.org/10.1103/PhysRevB.100.014418

John T, Scambelluri M, Frische M, Barnes JD, Bach W (2011) Dehydration of subducting serpentinite: implications for halogen mobility in subduction zones and the deep halogen cycle. Earth Planet Sci Lett 308:65–76. https://doi.org/10.1016/j.epsl.2011.05.038

Koemets E, Yuan L, Bykova E, Glazyrin K, Ohtani E, Dubrovinsky L (2020) Interaction between FeOOH and NaCl at extreme conditions: synthesis of novel $Na_2FeCl_4OH_x$ compound. Minerals 10:1–7. https://doi.org/10.3390/min10010051

Koemets E, Leonov I, Bykov M, Bykova E, Chariton S, Aprilis G, Fedotenko T, Clément S, Rouquette J, Haines J, Cerantola V, Glazyrin K, McCammon C, Prakapenka VB, Hanfland M, Liermann HP, Svitlyk V, Torchio R, Rosa AD, Irifune T, Ponomareva AV, Abrikosov IA, Dubrovinskaia N, Dubrovinsky L (2021) Revealing the complex nature of bonding in the binary high-pressure compound $FeO_2$. Phys Rev Lett 126:1–7. https://doi.org/10.1103/PhysRevLett.126.106001

Kurzydłowski D, Oleksiak A, Pillai SB, Jha PK (2020) High-pressure phase transitions of zinc difluoride up to 55 GPa. Inorg Chem 59:2584–2593. https://doi.org/10.1021/acs.inorgchem.9b03553

Lavina B, Dera P, Downs RT, Prakapenka V, Rivers M, Sutton S, Nicol M (2009) Siderite at lower mantle conditions and the effects of the pressure-induced spin-pairing transition. Geophys Res Lett 36:2–5. https://doi.org/10.1029/2009GL039652

Lin J, Speziale S, Mao Z, Marquardt H (2013) Effects of the electronic spin transitions of iron in lower mantle minerals: implications for deep mantle geophysics and geochemistry. Rev Geophys 51:244–275. https://doi.org/10.1002/rog.20010

Liu J, Hu Q, Kim DY, Wu Z, Wang W, Xiao Y, Chow P, Meng Y, Prakapenka VB, Mao H-K, Mao WL (2017) Hydrogen-bearing iron peroxide and the origin of ultralow-velocity zones. Nature 551:494–497. https://doi.org/10.1038/nature24461

Liu J, Hu Q, Bi W, Yang L, Xiao Y, Chow P, Meng Y, Prakapenka VB, Mao H-K, Mao WL (2019) Altered chemistry of oxygen and iron under deep earth conditions. Nat Commun 10:1–9. https://doi.org/10.1038/s41467-018-08071-3

Liu L, Yuan H, Yao Y, Yang Z, Gorelli FA, Giordano N, He L, Ohtani E, Zhang L (2022) Formation of an Al-rich niccolite-type silica in subducted oceanic crust: implications for water transport to the deep lower mantle. Geophys Res Lett 49:1–10. https://doi.org/10.1029/2021GL097178

Mao H-K, Hu Q, Yang L, Liu J, Kim DY, Meng Y, Zhang L, Prakapenka VB, Yang W, Mao WL (2017) When water meets iron at Earth's core-mantle boundary. Natl Sci Rev 4:870–878. https://doi.org/10.1093/nsr/nwx109

Merlini M, Hanfland M, Gemmi M, Huotari S, Simonelli L, Strobel P (2010) $Fe^{3+}$ spin transition in $CaFe_2O_4$ at high pressure. Am Mineral 95:200–203. https://doi.org/10.2138/am.2010.3347

Müller J, Speziale S, Efthimiopoulos I, Jahn S, Koch-Müller M (2016) Raman spectroscopy of siderite at high pressure: evidence for a sharp spin transition. Am Mineral 101:2638–2644. https://doi.org/10.2138/am-2016-5708

Nishi M, Kuwayama Y, Tsuchiya J, Tsuchiya T (2017) The pyrite-type high-pressure form of FeOOH. Nature 547:205–208. https://doi.org/10.1038/nature22823

Prescher C, Prakapenka VB (2015) High Press Res 35:223–230. https://doi.org/10.1080/08957959.2015.1059835. DIOPTAS: a program for reduction of two-dimensional X-ray diffraction data and data exploration

Roberge M, Bureau H, Bolfan-Casanova N, Raepsaet C, Surble S, Khodja H, Auzende AL, Cordier P, Fiquet G (2017) Chlorine in wadsleyite and ringwoodite: an experimental study. Earth Planet Sci Lett 467:99–107. https://doi.org/10.1016/j.epsl.2017.03.025

Rozenberg GK, Pasternak MP, Gorodetsky P, Xu WM, Dubrovinsky LS, Le Bihan T, Taylor RD (2009) Pressure-induced structural, electronic, and magnetic phase transitions in $FeCl_2$ studied by x-ray diffraction and resistivity measurements. Phys Rev B 79:1–7. https://doi.org/10.1103/PhysRevB.79.214105

Scambelluri M, Philippot P (2001) Deep fluids in subduction zones. Lithos 55:213–227. https://doi.org/10.1016/S0024-4937(00)00046-3

Streltsov SS, Shorikov AO, Skornyakov SL, Poteryaev AI, Khomskii DI (2017) Unexpected 3+ valence of iron in $FeO_2$, a geologically important material lying in between oxides and peroxides. Sci Rep 7:1–6. https://doi.org/10.1038/s41598-017-13312-4

Wirth R, Kaminsky F, Matsyuk S, Schreiber A (2009) Unusual micro- and nano-inclusions in diamonds from the Juina Area, Brazil. Earth Planet Sci Lett 286:292–303. https://doi.org/10.1016/j.epsl.2009.06.043

Yang Z, Yuan H, Liu L, Giordano N, Chen Y, Zhang L (2023) Chemical reaction between ferropericlase (Mg,Fe)O and water under high pressure-temperature conditions of the deep lower mantle. Am Mineral 108:530–535. https://doi.org/10.2138/am-2022-8390

Yin Y, Akbar FI, Bykova E, Aslandukova A, Laniel D, Aslandukov A, Bykov M, Han M, Garbarino G, Jia Z, Dubrovinsky L, Dubrovinskaia N (2022) Synthesis of rare-earth metal compounds through enhanced reactivity of alkali halides at high pressures. Commun Chem 5:1–7. https://doi.org/10.1038/s42004-022-00736-x

Yuan L, Ohtani E, Ikuta D, Kamada S, Tsuchiya J, Naohisa H, Ohishi Y, Suzuki A (2018) Chemical reactions between Fe and $H_2O$ up to megabar pressures and implications for water storage in the Earth's mantle and core. Geophys Res Lett 45:1330–1338. https://doi.org/10.1002/2017GL075720

Yuan H, Man L, Kim DY, Popov D, Meng Y, Greenberg E, Prakapenka V, Zhang L (2022) HP-$PdF_2$-type $FeCl_2$ as a potential Cl-carrier in the deep earth. Am Mineral 107:313–317. https://doi.org/10.2138/am-2022-8283

Zhang LL, Yan S, Jiang S, Yang K, Wang H, He SM, Liang DX, Zhang L, He Y, Lan XY, Mao CW, Wang J, Jiang H, Zheng Y, Dong ZH, Zeng LY, Li AG (2015) Hard X-ray micro-focusing beamline at SSRF. Nucl Sci Tech 26:1–8. https://doi.org/10.13538/j.1001-8042/nst.26.060101